Applied Physics Letters

Oxygen vacancies: The (in)visible friend of oxide electronics

Cite as: Appl. Phys. Lett. **116**, 120505 (2020); https://doi.org/10.1063/1.5143309
Submitted: 22 December 2019 • Accepted: 08 March 2020 • Published Online: 27 March 2020

F. Gunkel, D. V. Christensen, Y. Z. Chen, et al.

Applied Physics Letters PERSPECTIVE scitation.org/journal/apl

Oxygen vacancies: The (in)visible friend of oxide electronics

Cite as: Appl. Phys. Lett. **116**, 120505 (2020); doi: 10.1063/1.5143309
Submitted: 22 December 2019 · Accepted: 8 March 2020 ·
Published Online: 27 March 2020

F. Gunkel,[a] D. V. Christensen, Y. Z. Chen, and N. Pryds

AFFILIATIONS

Department of Energy Conversion and Storage, Technical University of Denmark, DK-2800 Kgs. Lyngby, Denmark

[a]Author to whom correspondence should be addressed: felgu@dtu.dk

ABSTRACT

Oxygen vacancies play crucial roles in determining the physical properties of metal oxides, representing important building blocks in many scientific and technological fields due to their unique chemical, physical, and electronic properties. However, oxygen vacancies are often invisible because of their dilute concentrations. Therefore, characterizing and quantifying their presence is of utmost importance for understanding and realizing functional metal oxide devices. This, however, is oftentimes a non-trivial task. In this Perspective paper, we discuss the relevant regimes of concentrations and associated phenomena arising from oxygen vacancies. We then focus on experimental techniques available for observing oxygen vacancies at widely different levels of concentrations. Finally, we discuss current challenges and opportunities for utilizing oxygen vacancies in metal oxides.

During the last few decades, it has been shown that many properties of solid materials are controlled not only by their geometry and electronic structure but also by functional defects and imperfections in their crystal structure.[1–7] The rapid progress in semiconductor nanotechnology, thus, relies on the control of materials themselves and on the success in understanding and controlling their defects.[1,2] In metal oxides, oxygen vacancies are one of the most common defects and are the subject of both theoretical and experimental research.[4–6] While oxygen vacancies are sometimes seen as detrimental to the properties of oxides, such as in dielectrics and some magnetic oxides, it has become apparent that oxygen vacancies can, in fact, induce new properties. Oxygen vacancies have been reported to drive insulating oxides into metals,[7] to drive nonmagnetic oxides toward magnetism,[8] to trigger superconductivity,[9,10] and to enhance catalytic activity[11] and ionic conductivity,[12–14] rendering them central players in oxide-based technologies employed in electronics and spintronics[10,15–19] as well as in energy harvesting and storage concepts (Fig. 1).[12,19–23] Exploiting and understanding oxygen vacancies, therefore, reflects a versatile strategy of designing functional properties of oxides by inducing and compensating for electronic charges through ionic defects. Oxygen vacancies can utilize new functionality: their presence facilitates oxygen ion diffusion in ionic devices (e.g., solid oxide fuel cells, electrolyzers, or gas separation membranes),[24–26] while their effect on the electronic structure is utilized in electronic applications such as field-effect devices, magnetoresitive devices, or spintronic devices.[17,18,27] Moreover, ionotronics reflects hybrid device concepts, which simultaneously harvest both ionic and electronic impacts of oxygen vacancies in oxides.[28] Important examples for this field are "valence change"-type memristive devices employing ionic motion to tailor electrical resistance for data storage and neuromorphic applications.[29–31] Other examples comprise oxygen exchange catalysts in electrolyzers and fuel cells or gas sensors. The borders between these different areas are rather gradual, and the distinction between ionic, ionotronic, and electronic phenomena is often not strict (Fig. 1).

Controlling and manipulating the defect structure provides a degree of freedom for harvesting and tailoring the functional properties of oxides. Oxygen vacancies are rather mobile ionic defects due to their comparably high diffusion coefficient, particularly at elevated temperature. For example, in $SrTiO_3$, the oxygen vacancy diffusion coefficient is about 10^{-6} cm^2/s at 900 K, so that oxygen vacancies can diffuse over micrometers in a few seconds.[6] Even at 300 K, the diffusion coefficient is still around 10^{-14} cm^2/s,[6] enabling vacancy diffusion on nanometer length scales.[32] This allows to tailor and control the properties resulting from oxygen vacancies in a dynamic manner via electric fields, temperature, pressure, or light by forming/healing defects or by moving and redistributing defects within the device.[3,29,33–43] This area, currently known as *defect engineering*, is

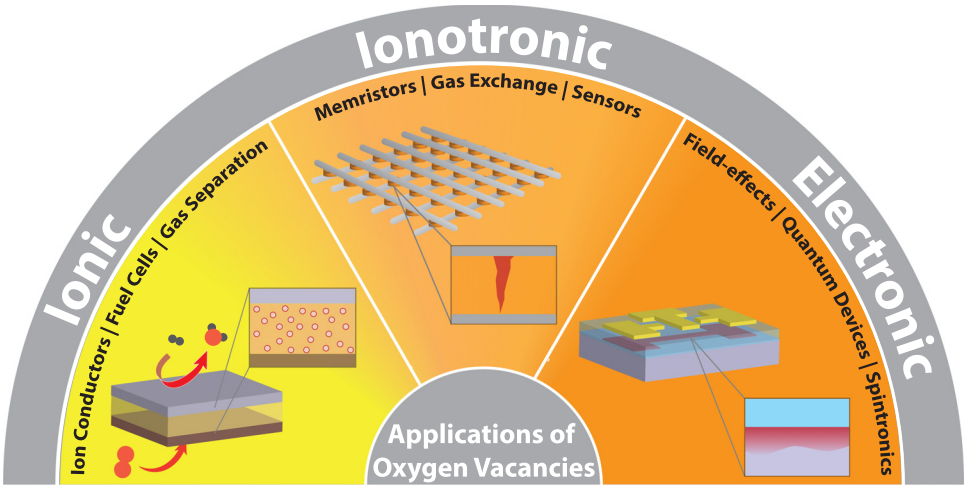

FIG. 1. Overview on relevant fields of research for oxygen-vacancy triggered phenomena and their applications in complex oxides. *Ionics* (left) employs oxygen ion diffusion arising from oxygen vacancies, e.g., in solid oxide fuel cells, electrolyzers, or gas separation membranes.[24–26] *Electronics* (right) utilizes the effect oxygen vacancies on the electronic structure of oxides, e.g., in field-effect devices, quantum devices, or spintronic devices.[17,18,27] *Ionotronics* (center) makes use of the coupled ionic and electronic phenomena arising from oxygen vacancies, such as in memristive devices, oxygen exchange catalysts, or gas sensors.

aimed at manipulating the nature and the concentration of defects in a material to tune its properties in a desired manner or to generate completely new and unexpected properties.[16,17]

The formation and annihilation of oxygen vacancies in transition metal oxides involves the dynamics of ionic defects, the exchange of oxygen from or into the surrounding, and the transfer of electronic charges from or into the material, rendering oxygen vacancy formation a complex solid-state redox-process.[4] Upon removal of oxygen, the two electrons formerly bound to the oxygen ion remain in the oxide and populate defect states, which in wide bandgap oxides are typically located inside the bandgap (in-gap states). When these donor states are shallow, the electrons can delocalize into the conduction band of the oxide, where they can conduct electricity in a nominally insulating material. Therefore, such *n*-type oxides can show an insulator-to-metal transition at a few ppm ($10^{16} - 10^{18}$ cm^{-3}) of oxygen vacancies and further enhanced conductivity at increased vacancy concentrations, such as that observed in the prototype oxide $SrTiO_3$.[7,44,45] On the other hand, *p*-type oxides typically show a metal-to-insulator transition at higher concentrations of oxygen vacancies as these reduce the hole concentration in the material. Some oxides can host oxygen-deficiency of up to tens of atomic percent, which can then yield phase transitions toward vacancy-ordered structures,[20,22,46] brownmillerite ($ABO_{2.5}$),[27,47,48] and infinite layer phases (ABO_2),[10] with a severe impact on the electronic structure of the oxide. In all cases, the local distribution of oxygen vacancies represents a fingerprint of the *chemical*, *crystallographic*, and *electronic* structure of the oxide.

At the atomic level, oxygen vacancies represent the lack of a few ions in a huge matrix of oxide material surrounding them. This often amounts to looking for the missing needle in the haystack. So how can we see these oxygen vacancies? The present methods to detect oxygen vacancies include advanced spectroscopy and advanced microscopy methods, complemented by classical defect chemical characterization, which probe oxygen vacancies through characteristic transport behaviors. Despite the recent advancements achieved in this direction, the research is still in the early stages. Thus, direct, rapid, and simple detection of oxygen vacancies is of great challenge owing to their elusive species and highly diluted contents. A complete understanding of the defect structure in these complex environments requires a variety of experimental approaches complemented by modeling and simulation tools.[49–53]

A central step in gaining the control over functional defects in oxides is the detailed understanding of their formation processes on the atomic scale. In this perspective paper, we will provide an overview on the state-of-the-art development in this intense research area with a focus on experimental techniques employed for probing the behavior of oxygen vacancies in complex oxides. Moreover, we will provide an indication of what is missing and where to go experimentally in the future.

The relevant concentrations of oxygen vacancy defects needed to observe defect-triggered phenomena in oxides typically vary over many orders of magnitude from the ppm region to tens of atomic percent. This poses great challenges toward experimental approaches to identify and characterize oxygen vacancy defects and their concentrations. At the same time, progressing miniaturization in state-of-the-art devices from bulk materials toward low dimensional structures, such as thin films and interfaces, results in the strong need to experimentally address oxygen vacancies not only in widely varying concentrations but also in confined dimensions. In Fig. 2, we summarize the typical concentrations of oxygen vacancies, accessible in different complex oxide materials (blue area), and link them to the typical defect-sensitivity of experimental techniques applied in the field in different regimes of concentrations (green area).

It is evident from the figure that classical techniques developed in the field of defect chemistry of oxides (light green area) are typically applicable to address very small concentrations of oxygen vacancies. During these measurements, however, the defect state of the sample is typically changed in order to derive characteristic behavior associated with low concentrations of oxygen vacancies. Moreover, these techniques are typically tailored for bulk samples. In contrast, advanced spectroscopy and state-of-the-art microscopy methods (dark green area) can probe defect concentrations and concentration profiles with nanoscale spatial resolution and even at the atomic level. However, these techniques often rely on rather high defect concentrations (typically of order of 1 at. %). They are, hence, insensitive to defect concentrations at the ppm level, resulting in a considerable gap between the defect concentrations that induce electronic phenomena and experimentally accessible chemical information.

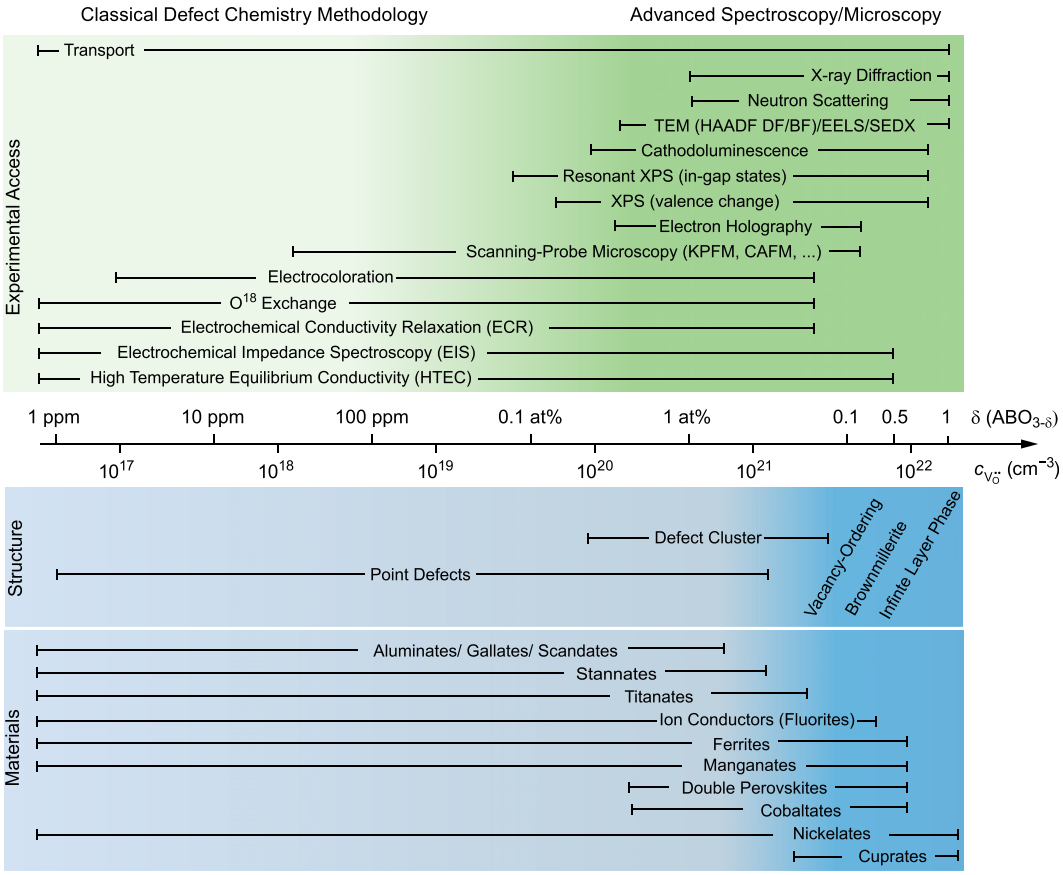

FIG. 2. Experimental methods available to probe oxygen vacancies on different orders of magnitude in concentration (green color) and occurrence of vacancies in different materials systems (blue color).

In the following, we will discuss in more detail the experimental techniques available to probe oxygen vacancy concentrations, starting with very dilute concentrations in the ppm regime and moving toward larger concentrations, and link the concentration regimes to typical physical phenomena and properties observed in complex oxides at corresponding concentrations. We note that the discussed methods typically *do not* probe directly the actual vacancy site in the oxide but link a measurable and experimentally accessible property of the oxide to the presence of oxygen vacancies. Therefore, characterizing oxygen vacancies relies on a careful data analysis and assessment of model assumptions when converting experimental results into the effective vacancy concentration. The model assumptions used for data analysis often require further assessment either from auxiliary experiments or from theory calculations, which are sometimes even essential to the raw data analysis (e.g., to predict the energy levels of defect states), rendering the analysis of oxygen vacancy concentrations a non-trivial task.

At low concentrations of oxygen vacancies ($c_{V_O^{\cdot\cdot}} < 10^{19}\,\mathrm{cm}^{-3}$), oxygen vacancies can typically not be detected by probing the absolute oxygen content of the oxide by chemical or spectroscopic means. Instead, electrical transport measurements can be used to probe oxygen vacancies indirectly. In the simplest case, Hall measurements can yield the concentration of oxygen vacancies from the electronic carrier density, assuming that each oxygen vacancy provides a known number of conducting electrons. This is the case in most *n*-type insulting oxides such as $SrTiO_3$ where the electron concentration results from doubly ionized oxygen vacancies ($c_{V_O^{\cdot\cdot}} = n/2$).[54] This, however, holds only if the electrons do not become localized or compensated by other ionic defects. Close to the impurity level, the electron density, therefore, typically departs from this simple relation as impurity compensation results in additional oxygen vacancies without adding electronic charges to the system.[54,55] Moreover, oxygen vacancies can give rise to localized electronic states, not contributing to the electronic transport and affecting the estimation of oxygen vacancy concentrations, particularly in the low carrier density regime.[56]

Oxides that are insulating without the presence of oxygen vacancies can show a transition into metallic behavior when inducing oxygen vacancies at ppm concentrations. For $SrTiO_3$, a threshold for metallic behavior was observed at about $1 \times 10^{17}\,\mathrm{cm}^{-3}$ carriers,[57] close to the typical impurity level of $SrTiO_3$ single crystals. Likewise, for stannates, an insulator-to-metal transition was observed at a carrier concentration of about $1 \times 10^{18}\,\mathrm{cm}^{-3}$.[58–60] In contrast, aluminates, gallates, or scandates typically show electronically insulating behavior. In those cases, the oxygen vacancy concentration is determined merely

by the impurity level (or intentional acceptor-doping).[61–65] Ferrites show a strong change in color in the low concentration regime owing to the varying valence state of iron with increasing amount of oxygen vacancies (electrocoloration).[66] *p*-type conducting oxides, such as mixed A-site manganites, cobaltates, and nickelates, are typically less sensitive to low concentrations of oxygen vacancy defects due to their large carrier densities, making the determination of oxygen vacancy defects from transport difficult.

In all these cases, the oxygen vacancies themselves remain *invisible* and need to be addressed via indirect probes and modeling. Classical defect chemistry methodologies such as high temperature equilibrium conductivity (HTEC),[55,67–69] impedance spectroscopy,[70–72] electrochemical conductivity relaxation (ECR),[43,73] O^{18} exchange,[74–76] and electrocoloration[66,77,78] employ the characteristic behavior of electronic-ionic conductivity (and/or optical properties) on a variation of the oxygen chemical potential. For example, electrical conductivity is measured in equilibrium with the surrounding atmosphere at different oxygen partial pressures. The concentrations of electronic and ionic carriers can then be modeled based on chemical equilibria of solid-state redox-reactions.[54] Such a rigorous thermodynamic modeling allows us to extract defect concentrations as well as inherent impurity levels.[54,74,79] This strategy, however, requires to expose the sample to elevated temperature and varying oxygen atmosphere which implies an active change of the original defect state. Moreover, these techniques carried out at high temperatures typically require macroscopic samples. Only very recent studies applied these methodologies to confined oxide electronic systems, thin films, and interfaces by introducing appropriate substrate correction[68,69] and space charge models of the thermodynamic processes.[79–81]

Advanced spectroscopy and microscopy methods are often not sensitive enough in the ppm-regime to chemically probe oxygen vacancies or the associated valence change of the transition metal directly. Spectroscopic determination of the absolute positions of the Fermi level with respect to the valence band/core levels or photoluminsence,[82,83] however, can give additional insights into the electronic structure and doping concentration.

Approaching the intermediate concentration regime (10^{19} cm^{-3} $< c_{V_O^{\bullet\bullet}} < 10^{21}$ cm^{-3}), oxygen vacancies become accessible to techniques that probe the valence state of the transition metal as well as oxygen content and chemical environment of atoms directly. These techniques then allow us to address and image oxygen vacancies spectroscopically and microscopically. The valence state of transition metals may be probed via photoemission or x-ray absorption techniques, whereas the chemical environment and chemical bonds can be accessed in the O–K absorption edge in the transition metal absorption spectra[21,84,85] and their extended fine structure (EXAFS). Sensitivity can be enhanced by applying resonant techniques such as resonant XPS yielding access to in-gap states in wide bandgap oxides.[86,87] Further techniques comprise Raman spectroscopy[88] or electron paramagnetic resonance (EPR).[89–91] Spectroscopy can also be combined with microscopy techniques, based on electron transmission (TEM), including dark-field[92] and bright-field imaging,[93,94] to image oxygen (vacancies) in direct imaging contrast. Care has to be taken, however, as microscopic contrast can be obtained not only by oxygen vacancies but also by other types of defects, such as chemical intermixing[95] or cation vacancies,[96,97] both particularly important in thin films and heterostructures of complex oxides. Therefore, a combination of imaging and chemical analysis is required to unambiguously identify oxygen vacancies. In this intermediate concentration regime, oxygen vacancies are often at the edge of becoming *visible*. Electronically, however, it can still be a challenge to decouple the effect of oxygen vacancies from other competing phenomena, such as in the case of $SrTiO_3$-based 2DEG systems: These exist at comparably low carrier concentrations ($\lesssim 10^{19}$ cm^{-3}), where electronic phenomena such as metal-insulator transitions,[42,98,99] superconductivity,[100,101] and magnetic reconstructions[8,102–104] were observed and at higher carrier concentrations ($\gtrsim 10^{20}$ cm^{-3}) where the presence of oxygen vacancies becomes accessible microscopically and spectroscopically. In the transition between these two regimes, however, the question to which extent electronic charge-transfer and ionic (oxygen vacancy related) generation of carriers dominates the properties remains open.[82,105]

Oxygen vacancy-related phenomena in the similar concentration range (10^{19} cm^{-3} – 10^{21} cm^{-3}) furthermore comprise the formation of conducting filaments in memristive devices, where the oxygen vacancy concentration is typically exceeding thermodynamic concentrations and can be as high as 10^{21} cm^{-3}.[106] Under these concentrations, the local oxygen concentration as well as electron concentration can be probed using microscopic measurements such electron holography and electron energy loss spectroscopy.[83,106] Moreover, scanning probe techniques become capable of detecting local changes in electrical conductivity caused by oxygen vacancies (conductive-tip atomic force microscopy/C-AFM)[107] or local contrast in work function (Kelvin-probe AFM)[32,41,108] or optical properties (scanning near-field optical spectroscopy/SNOM)[109,110] either in surface scanning or cross-sectional geometry. For these scanning probe techniques lower defect concentrations may also be probed when a good reference is available for direct comparison.

A further increase in the vacancy concentration above 10^{21} cm^{-3} leads to strong interactions between defects:[51,111] defect-clustering and defect-ordering in defined structures are observed, eventually driving the material toward phase transitions. In many oxides, however, such as in the case of $SrTiO_3$, very high oxygen vacancy concentrations in the range of 10^{21} cm^{-3} $< c_{V_O^{\bullet\bullet}} < 10^{22}$ cm^{-3} are hard to be achieved thermodynamically, e.g., by vacuum annealing[44,57,112] or annealing in chemically reducing atmospheres (hydrogen-derived atmospheres).[39,55,97,109,113] In those cases, such high concentrations may be accessible via extreme extrinsic doping or chemical substitution,[114] such as employed in ion-conductors like yttria-stabilized zirconia (YSZ).[12,19,24,115] Furthermore, interfacial redox reactions, such as in the case of $SrTiO_3$-based heterostructures[116,117] and soft-chemistry topotactic reduction using reduction agents such as CaH_2[10] can result in high concentrations of oxygen vacancies.

The thermodynamic driving force required for inducing high amounts of oxygen is related to the valence state of the transition metal. Therefore, cobaltates (preferred Co valence state of 3+/2+ in the perovskite structure) allow more oxygen vacancies to be formed under similar thermodynamic conditions than manganites and ferrites (4+/3+/2+) or titanates (4+/3+). The lower the preferred valence state, the more the material is prone to induce oxygen vacancies also at the level of tens of atomic percent. Additionally, a mixed A-site composition with lower-valent cations can further support the formation of oxygen vacancies. As a result, oxygen-vacancy ordering phenomena, double-perovskite formation, as well as brownmillerite phases can be obtained in cobaltates (with $SrCoO_{2.5}$ being the most important example),[47] and also $SrFeO_{3-\delta}$[48] and (La,Sr)$MnO_{3-\delta}$[118,119] have been

shown to form vacancy-ordered phases and a brownmillerite structure. Brownmillerite phases are of high interest for tailoring catalytic properties[20,22] and ionic conductivity as they potentially provide defined diffusion paths for oxygen migration.[120] The phase transition is moreover often accompanied by a metal–insulator transition utilized in memristive devices.[47,48] An even more extreme phase transition has been reported for nickelates, which undergo a phase transition into an infinite-layer-type phase, similar to cuprates ($ACuO_2$). While nickelates in the perovskite structure typically show metallic behavior around room temperature and a temperature-induced metal–insulator transition, the infinite layer phase has been shown to become superconducting upon doping, promising to allow to tailor superconductivity in nickelates in a similar manner as in high-T_C cuprate superconductors.[10] In those cases, the materials undergo a phase transition, where the former point defects become a regular constituent of the new structure. This picture implies that such phase transitions may be controlled chemically, i.e., by starting from an oxygen-deficient perovskite structure and driving the phase transition by further reducing the oxygen content in the oxide.

In the high-concentration regime ($10^{21}\,cm^{-3} \lesssim c_{V_O^{\cdot\cdot}} \lesssim 10^{22}\,cm^{-3}$), oxygen-vacancies are well resolved in atomic imaging techniques and characteristic signatures arising from oxygen vacancies can be observed in x-ray absorption. Also neutron scattering (sensitive to lattice occupations) has sufficient sensitivity to determine the absolute vacancy concentration.[118] Even more, standard lab-tools like x-ray diffraction (XRD) become accessible to detect vacancy concentrations: high amounts of oxygen-vacancies typically yield lattice expansion related to the change in ionic radius of the transition metal in different valence states as well as Coulomb repulsion of unscreened cations detectible in the lattice spacing of the oxide.[121] Moreover, defect-ordering and phase transitions can give rise to superstructure reflections observed in lab-XRD and in TEM-based electron diffraction or synchrotron-based x-ray diffraction experiments.[22,46] While spectroscopic signatures are often still complex to be assigned and understood in terms of ordering and phase transitions, direct and simple evidence through imaging and diffraction is accessible in this high concentration regime, facilitating to link electronic phenomena to the associated oxygen vacancy defect structure. Oxygen vacancies are, thus, *visible* in this regime. Obviously, the phenomena described in this section go well beyond point defect formation and have a severe impact even on the lattice and crystal structure of the oxide, making oxygen vacancies easily accessible in these materials. As discussed above, however, oxygen vacancies can be effective at much lower concentration ($\lesssim 10^{19}\,cm^{-3}$), where it becomes a real challenge to observe them directly, opening a gap between accessible experimental techniques, relevant defect concentration, and desired application.

As a future perspective, oxygen vacancies remain one of the most fundamental and fascinating ionic species in the field of complex oxides—sometimes desired to drive functionality and sometimes unwanted when crystal perfection is the goal. The particular challenge in the field lies in the fact that concentrations of defects that are *invisible* can already have a severe impact on the properties of oxides. In those cases, defect-structure–property relations can only be addressed indirectly and often in a disruptive manner that affects the sample state itself. As for large concentrations, various techniques become available to make oxygen vacancies *visible*, but there remains a considerable gap between the relevant defect concentration, available experimental techniques, and observed phenomena in the diluted limit ($\lesssim 10^{19}\,cm^{-3}$). In Fig. 2, these oxide systems would group in the center or left concentration range, where fundamentally interesting phenomena such as metal-insulator transitions occur. Hence, there is a huge demand for developing techniques that allow us to probe smaller concentrations, with larger spatial accuracy, and potentially during the dynamic variation of the defect level. One approach toward combining state-of-the-art spectroscopy/microscopy and classical defect chemical pO_2-dependencies is the ambient pressure and environmental techniques available for photoemission spectroscopy or transmission electron microscopy.[73,122–126] These allow us to combine classical (thermodynamic) characterization and advanced methodology to benefit from both expanded sensitivity toward low concentrations and spatial resolution. In situ and in operando techniques also bear huge potential for the understanding of oxide electronic devices during operation.[106,119,127] Currently, we are lacking the sensitivity to resolve oxygen vacancies within the low concentration range required for important functionality such as the oxygen vacancy-driven metal–insulator-transitions in wide bandgap insulators or at functional heterointerfaces and memristive devices. Further progress, in both experimental and theoretical methodology, will be key in developing and controlling nanoionic-electronic devices based on complex oxides.

F.G. thanks funding from the European Union's Horizon 2020 research and innovation program under Marie Sklodowska-Curie Grant Agreement No. 713683 (COFUNDfellowsDTU). N.P. and D.V.C. would like to thank the support from the Independent Research Fund Denmark, Grant No. 6111-00145B. N.P. furthermore is thankful for support from the BioWings project funded by the European Union's Horizon 2020, Future and Emerging Technologies (FET) programme (Grant No. 801267). Y.Z.C. thanks the support from the Independent Research Fund Denmark, Grant No. 9041-00034B.

REFERENCES

[1]H. J. Queisser and E. E. Haller, Science **281**, 945 (1998).
[2]S. T. Pantelides, Rev. Mod. Phys. **50**, 797 (1978).
[3]R. Waser and M. Aono, Nat. Mater. **6**, 833 (2007).
[4]R. Merkle and J. Maier, Angew. Chem., Int. Ed. **47**, 3874 (2008).
[5]M. V. Ganduglia-Pirovano, A. Hofmann, and J. Sauer, Surf. Sci. Rep. **62**, 219 (2007).
[6]R. A. De Souza, Adv. Funct. Mater. **25**, 6326 (2015).
[7]O. N. Tufte and P. W. Chapman, Phys. Rev. **155**, 796 (1967).
[8]M. Salluzzo, S. Gariglio, D. Stornaiuolo, V. Sessi, S. Rusponi, C. Piamonteze, G. M. De Luca, M. Minola, D. Marré, A. Gadaleta, H. Brune, F. Nolting, N. B. Brookes, and G. Ghiringhelli, Phys. Rev. Lett. **111**, 087204 (2013).
[9]C. W. Rischau, X. Lin, C. P. Grams, D. Finck, S. Harms, J. Engelmayer, T. Lorenz, Y. Gallais, B. Fauqué, J. Hemberger, and K. Behnia, Nat. Phys. **13**, 643 (2017).
[10]D. Li, K. Lee, B. Y. Wang, M. Osada, S. Crossley, H. R. Lee, Y. Cui, Y. Hikita, and H. Y. Hwang, Nature **572**, 624 (2019).
[11]A. Grimaud, O. Diaz-Morales, B. Han, W. T. Hong, Y.-L. Lee, L. Giordano, K. A. Stoerzinger, M. T. M. Koper, and Y. Shao-Horn, Nat. Chem. **9**, 457 (2017).
[12]J. Garcia-Barriocanal, A. Rivera-Calzada, M. Varela, Z. Sefrioui, E. Iborra, C. Leon, S. J. Pennycook, and J. Santamaria, Science **321**, 676 (2008).
[13]S. Sanna, V. Esposito, A. Tebano, S. Licoccia, E. Traversa, and G. Balestrino, Small **6**, 1863 (2010).
[14]S. Sanna, V. Esposito, J. W. Andreasen, J. Hjelm, W. Zhang, T. Kasama, S. B. Simonsen, M. Christensen, S. Linderoth, and N. Pryds, Nat. Mater. **14**, 500 (2015).

[15]D. G. Schlom and J. Mannhart, Nat. Mater. **10**, 168 (2011).
[16]H. Y. Hwang, Y. Iwasa, M. Kawasaki, B. Keimer, N. Nagaosa, and Y. Tokura, Nat. Mater. **11**, 103 (2012).
[17]D. Christensen, F. Trier, W. Niu, Y. Gan, Y. Zhang, T. Jespersen, Y. Chen, and N. Pryds, Adv. Mater. Interfaces **6**, 1900772 (2019).
[18]M. Bibes, J. E. Villegas, and A. Barthelemy, Adv. Phys. **60**, 5 (2011).
[19]N. H. Pryds and V. Esposito, J. Electroceram. **38**, 1 (2017).
[20]A. Grimaud, K. J. May, C. E. Carlton, Y. lin Lee, M. Risch, W. T. Hong, J. Zhou, and Y. Shao-Horn, Nat. Commun. **4**, 2439 (2013).
[21]D. N. Mueller, M. L. Machala, H. Bluhm, and W. C. Chueh, Nat. Commun. **6**, 6097 (2015).
[22]F. Gunkel, L. Jin, D. N. Mueller, C. Hausner, D. S. Bick, C.-L. Jia, T. Schneller, I. Valov, R. Waser, and R. Dittmann, ACS Catal. **7**, 7029 (2017).
[23]M. L. Weber, C. Baeumer, D. N. Mueller, L. Jin, C.-L. Jia, D. S. Bick, R. Waser, R. Dittmann, I. Valov, and F. Gunkel, Chem. Mater. **31**, 2337 (2019).
[24]A. Tarancon, M. Burriel, J. Santiso, S. J. Skinner, and J. A. Kilner, J. Mater. Chem. **20**, 3799 (2010).
[25]S. J. Skinner and J. A. Kilner, Mater. Today **6**, 30 (2003).
[26]M. Mogensen, D. Lybye, N. Bonanos, P. Hendriksen, and F. Poulsen, Solid State Ionics **174**, 279 (2004).
[27]Y. Chen, R. Green, R. Sutarto, F. He, S. Linderoth, G. Sawatzky, and N. Pryds, Nano Lett. **17**, 7062 (2017).
[28]D. D. Fong and S. Ramanathan, APL Mater. **5**, 042201 (2017).
[29]R. Waser, R. Dittmann, G. Staikov, and K. Szot, Adv. Mater. **21**, 2632 (2009).
[30]R. Dittmann and J. P. Strachan, APL Mater. **7**, 110903 (2019).
[31]S. Lee, A. Sangle, P. Lu, A. Chen, W. Zhang, J. S. Lee, H. Wang, Q. Jia, and J. L. MacManus-Driscoll, Adv. Mater. **26**, 6284 (2014).
[32]M. Andrä, F. Gunkel, C. Bäumer, C. Xu, R. Dittmann, and R. Waser, Nanoscale **7**, 14351 (2015).
[33]Y. Li, S. Sanna, K. Norrman, D. V. Christensen, C. S. Pedersen, J. M. Garcia Lastra, and N. Pryds, Appl. Surf. Sci. **470**, 1071 (2019).
[34]C. Baeumer, N. Raab, T. Menke, C. Schmitz, R. Rosezin, P. M. Müller, M. Andrä, V. Feyer, R. Bruchhaus, F. Gunkel, C. M. Schneider, R. Waser, and R. Dittmann, Nanoscale **8**, 13967 (2016).
[35]C. Baeumer, C. Xu, F. Gunkel, N. Raab, R. A. Heinen, A. Koehl, and R. Dittmann, Sci. Rep. **5**, 11829 (2015).
[36]C. Leighton, Nat. Mater. **18**, 13 (2019).
[37]N. Lu, P. Zhang, Q. Zhang, R. Qiao, Q. He, H.-B. Li, Y. Wang, J. Guo, D. Zhang, Z. Duan, Z. Li, M. Wang, S. Yang, M. Yan, E. Arenholz, S. Zhou, W. Yang, L. Gu, C.-W. Nan, J. Wu, Y. Tokura, and P. Yu, Nature **546**, 124 (2017).
[38]D. Christensen, Y. Frenkel, Y. Xie, Z. Chen, Y. Hikita, A. Smith, Y. Chen, L. Klein, H. Hwang, N. Pryds, and B. Kalisky, Nat. Phys. **15**, 269 (2019).
[39]C. Xu, C. Bäumer, R. A. Heinen, S. Hoffmann-Eifert, F. Gunkel, and R. Dittmann, Sci. Rep. **6**, 22410 (2016).
[40]S. Thiel, G. Hammerl, A. Schmehl, C. W. Schneider, and J. Mannhart, Science **313**, 1942 (2006).
[41]F. Hensling, D. J. Keeble, J. Zhu, S. Brose, C. Xu, F. Gunkel, S. Danylyuk, S. S. Nonnenmann, W. Egger, and R. Dittmann, Sci. Rep. **8**, 8846 (2018).
[42]M. von Soosten, D. Christensen, C.-B. Eom, T. Jespersen, Y. Chen, and N. Pryds, Sci. Rep. **9**, 18005 (2019).
[43]A. Viernstein, M. Kubicek, M. Morgenbesser, G. Walch, G. C. Brunauer, and J. Fleig, Adv. Funct. Mater. **29**, 1900196 (2019).
[44]H. P. R. Frederikse and W. R. Hosler, Phys. Rev. **161**, 822 (1967).
[45]R. Moos and K. H. Haerdtl, J. Appl. Phys. **80**, 393 (1996).
[46]C. Frontera, A. Caneiro, A. E. Carrillo, J. Oro-Sole, and J. L. Garcia-Munoz, Chem. Mater. **17**, 5439 (2005).
[47]H. Jeen, W. S. Choi, J. W. Freeland, H. Ohta, C. U. Jung, and H. N. Lee, Adv. Mater. **25**, 3651 (2013).
[48]V. R. Nallagatla, T. Heisig, C. Baeumer, V. Feyer, M. Jugovac, G. Zamborlini, C. M. Schneider, R. Waser, M. Kim, C. U. Jung, and R. Dittmann, Adv. Mater. **31**, 1903391 (2019).
[49]A. OHara, G. Bersuker, and A. A. Demkov, J. Appl. Phys. **115**, 183703 (2014).
[50]A. F. Zurhelle, X. Tong, A. Klein, D. S. Mebane, and R. A. D. Souza, Angew. Chem., Int. Ed. **56**, 14516–14520 (2017).
[51]M. Schie, S. Menzel, J. Robertson, R. Waser, and R. A. D. Souza, Phys. Rev. Mater. **2**, 035002 (2018).
[52]E. Abbaspour, S. Menzel, A. Hardtdegen, S. Hoffmann-Eifert, and C. Jungemann, IEEE Trans. Nanotechnol. **17**, 1181 (2018).
[53]C. Funck and S. Menzel, AIP Adv. **9**, 045116 (2019).
[54]D. M. Smyth, *The Defect Chemistry of Metal Oxides* (Oxford University Press, 2000).
[55]R. Moos and K. H. Hardtl, J. Am. Ceram. Soc. **80**, 2549 (1997).
[56]F. Trier, D. V. Christensen, and N. Pryds, J. Phys. D **51**, 293002 (2018).
[57]A. Spinelli, M. A. Torija, C. Liu, C. Jan, and C. Leighton, Phys. Rev. B **81**, 155110 (2010).
[58]K. Ganguly, A. Prakash, B. Jalan, and C. Leighton, APL Mater. **5**, 056102 (2017).
[59]A. Prakash, P. Xu, A. Faghaninia, S. Shukla, J. W. Ager, C. S. Lo, and B. Jalan, Nat. Commun. **8**, 15167 (2017).
[60]H. Paik, Z. Chen, E. Lochocki, S. H. Ariel, A. Verma, N. Tanen, J. Park, M. Uchida, S. Shang, B.-C. Zhou, M. Bruetzam, R. Uecker, Z.-K. Liu, D. Jena, K. M. Shen, D. A. Muller, and D. G. Schlom, APL Mater. **5**, 116107 (2017).
[61]T. Ishihara, H. Matsuda, and Y. Takita, J. Am. Chem. Soc. **116**, 3801 (1994).
[62]A. Petric and P. Huang, Solid State Ionics **92**, 113 (1996).
[63]S. Tidrow, W. Wilber, A. Tauber, S. Schauer, D. Eckart, R. Finnegan, and R. Pfeffer, J. Mater. Res. **10**, 1622 (1995).
[64]T. Ishihara, H. Matsuda, M. A. bin Bustam, and Y. Takita, in Proceedings of the 10th International Conference on Solid State Ionics [Solid State Ionics **86-88**(Part 1), 197 (1996)].
[65]T. L. Nguyen, Solid State Ionics **130**, 229 (2000).
[66]N. H. Perry, J. J. Kim, and H. L. Tuller, Sci. Technol. Adv. Mater. **19**, 130 (2018).
[67]R. Waser, J. Am. Ceram. Soc. **74**, 1934 (1991).
[68]F. Gunkel, S. Hoffmann-Eifert, R. Dittmann, S. Mi, C. Jia, P. Meuffels, and R. Waser, Appl. Phys. Lett. **97**, 012103 (2010).
[69]F. Gunkel, P. Brinks, S. Hoffmann-Eifert, R. Dittmann, M. Huijben, J. E. Kleibeuker, G. Koster, G. Rijnders, and R. Waser, Appl. Phys. Lett. **100**, 052103 (2012).
[70]F. S. Baumann, J. Fleig, H.-U. Habermeier, and J. Maier, Solid State Ionics **177**, 1071 (2006).
[71]M. Kubicek, T. M. Huber, A. Welzl, A. Penn, G. M. Rupp, J. Bernardi, M. Stöger-Pollach, H. Hutter, and J. Fleig, Solid State Ionics **256**, 38 (2014).
[72]J. Fleig, J. Electroceram. **13**, 637 (2004).
[73]M. Andrä, H. Bluhm, R. Dittmann, C. M. Schneider, R. Waser, D. N. Mueller, and F. Gunkel, Phys. Rev. Mater. **3**, 044604 (2019).
[74]R. A. De Souza, Phys. Chem. Chem. Phys. **11**, 9939 (2009).
[75]R. A. De Souza, V. Metlenko, D. Park, and T. E. Weirich, Phys. Rev. B **85**, 174109 (2012).
[76]V. Metlenko, A. Ramadan, F. Gunkel, H. Du, H. Schraknepper, S. Hoffmann-Eifert, R. Dittmann, R. Waser, and R. D. Souza, Nanoscale **6**, 12864 (2014).
[77]R. Waser, T. Baiatu, and K.-H. Härdtl, J. Am. Ceram. Soc. **73**, 1654 (1990).
[78]V. Havel, A. Marchewka, S. Menzel, S. Hoffmann-Eifert, G. Roth, and R. Waser, MRS Proc. **1691**, mrss14 (2014).
[79]R. A. D. Souza, F. Gunkel, S. Hoffmann-Eifert, and R. Dittmann, Phys. Rev. B **89**, 241401(R) (2014).
[80]F. Gunkel, R. Waser, A. H. H. Ramadan, R. A. De Souza, S. Hoffmann-Eifert, and R. Dittmann, Phys. Rev. B **93**, 245431 (2016).
[81]F. Baiutti, G. Logvenov, G. Gregori, G. Cristiani, Y. Wang, W. Sigle, P. A. van Aken, and J. Maier, Nat. Commun. **6**, 8586 (2015).
[82]A. Kalabukhov, R. Gunnarsson, J. Borjesson, E. Olsson, T. Claeson, and D. Winkler, Phys. Rev. B **75**, 121404 (2007).
[83]H. Lee, N. Campbell, J. Lee, T. J. Asel, T. R. Paudel, H. Zhou, J. W. Lee, B. Noesges, J. Seo, B. Park, L. J. Brillson, S. H. Oh, E. Y. Tsymbal, M. S. Rzchowski, and C. B. Eom, Nat. Mater. **17**, 231–236 (2018).
[84]C. Baeumer, C. Schmitz, A. H. H. Ramadan, H. Du, K. Skaja, V. Feyer, P. Müller, B. Arndt, C.-L. Jia, J. Mayer, R. A. De Souza, C. Michael Schneider, R. Waser, and R. Dittmann, Nat. Commun. **6**, 8610 (2015).
[85]C. Baeumer, C. Schmitz, A. Marchewka, D. N. Mueller, R. Valenta, J. Hackl, N. Raab, S. P. Rogers, M. I. Khan, S. Nemsak, M. Shim, S. Menzel, C. M. Schneider, R. Waser, and R. Dittmann, Nat. Commun. **7**, 12398 (2016).
[86]C. Baeumer, C. Funck, A. Locatelli, T. O. Mentes, F. Genuzio, T. Heisig, F. Hensling, N. Raab, C. M. Schneider, S. Menzel, R. Waser, and R. Dittmann, Nano Lett. **19**, 54 (2019).

[87]P. Schütz, D. V. Christensen, V. Borisov, F. Pfaff, P. Scheiderer, L. Dudy, M. Zapf, J. Gabel, Y. Z. Chen, N. Pryds, V. A. Rogalev, V. N. Strocov, C. Schlueter, T.-L. Lee, H. O. Jeschke, R. Valentí, M. Sing, and R. Claessen, Phys. Rev. B **96**, 161409 (2017).
[88]F. Pfaff, H. Fujiwara, G. Berner, A. Yamasaki, H. Niwa, H. Kiuchi, A. Gloskovskii, W. Drube, J. Gabel, O. Kirilmaz, A. Sekiyama, J. Miyawaki, Y. Harada, S. Suga, M. Sing, and R. Claessen, Phys. Rev. B **97**, 035110 (2018).
[89]S. Lenjer, O. F. Schirmer, H. Hesse, and T. W. Kool, Phys. Rev. B **66**, 165106 (2002).
[90]K. Blazey, R. Koch, and K. Mueller, Mater. Res. Bull. **16**, 1149 (1981).
[91]D. J. Keeble, Z. Li, and E. H. Poindexter, J. Phys.: Condens. Matter **7**, 6327 (1995).
[92]A. Ohtomo, D. A. Muller, J. L. Grazul, and H. Y. Hwang, Nature **419**, 378 (2002).
[93]V. Srot, Y. Wang, M. Minola, M. Salluzzo, G. M. De Luca, B. Keimer, and P. A. van Aken, Microsc. Microanal. **24**, 76 (2018).
[94]V. Srot, Y. Wang, M. Minola, U. Salzberger, M. Salluzzo, G. M. De Luca, B. Keimer, and P. A. van Aken, Microsc. Microanal. **25**, 1750 (2019).
[95]N. Nakagawa, H. Y. Hwang, and D. A. Muller, Nat. Mater. **5**, 204 (2006).
[96]D. J. Keeble, S. Wicklein, L. Jin, C. L. Jia, W. Egger, and R. Dittmann, Phys. Rev. B **87**, 195409 (2013).
[97]F. Gunkel, S. Wicklein, P. Brinks, S. Hoffmann-Eifert, M. Huijben, G. Rijnders, R. Waser, and R. Dittmann, Nanoscale **7**, 1013 (2015).
[98]G. Herranz, M. Basletic, M. Bibes, C. Carretero, E. Tafra, E. Jacquet, K. Bouzehouane, C. Deranlot, A. Hamzic, J. M. Broto, A. Barthelemy, and A. Fert, Phys. Rev. Lett. **98**, 216803 (2007).
[99]O. Copie, V. Garcia, C. Bodefeld, C. Carretero, M. Bibes, G. Herranz, E. Jacquet, J.-L. Maurice, B. Vinter, S. Fusil, K. Bouzehouane, H. Jaffres, and A. Barthelemy, Phys. Rev. Lett. **102**, 216804 (2009).
[100]N. Reyren, S. Thiel, A. D. Caviglia, L. F. Kourkoutis, G. Hammerl, C. Richter, C. W. Schneider, T. Kopp, A.-S. Ruetschi, D. Jaccard, M. Gabay, D. A. Muller, J. M. Triscone, and J. Mannhart, Science **317**, 1196 (2007).
[101]A. D. Caviglia, S. Gariglio, N. Reyren, D. Jaccard, T. Schneider, M. Gabay, S. Thiel, G. Hammerl, J. Mannhart, and J. M. Triscone, Nature **456**, 624 (2008).
[102]A. Brinkman, M. Huijben, M. V. Zalk, J. Huijben, U. Zeitler, J. C. Maan, W. G. V. der Wiel, G. Rijnders, D. H. A. Blank, and H. Hilgenkamp, Nat. Mater. **6**, 493 (2007).
[103]J. S. Lee, Y. W. Xie, H. K. Sato, C. Bell, Y. Hikita, H. Y. Hwang, and C. C. Kao, Nat. Mater. **12**, 703 (2013).
[104]F. Gunkel, C. Bell, H. Inoue, B. Kim, A. G. Swartz, T. A. Merz, Y. Hikita, S. Harashima, H. K. Sato, M. Minohara, S. Hoffmann-Eifert, R. Dittmann, and H. Y. Hwang, Phys. Rev. X **6**, 031035 (2016).
[105]F. Gunkel, S. Hoffmann-Eifert, R. A. Heinen, D. V. Christensen, Y. Z. Chen, N. Pryds, R. Waser, and R. Dittmann, ACS Appl. Mater. Interfaces **9**, 1086 (2017).
[106]D. Cooper, C. Baeumer, N. Bernier, A. Marchewka, C. L. Torre, R. E. Dunin-Borkowski, S. Menzel, R. Waser, and R. Dittmann, Adv. Mater. **29**, 1700212 (2017).
[107]R. Muenstermann, T. Menke, R. Dittmann, and R. Waser, Adv. Mater. **22**, 4819 (2010).
[108]J. Zhu, J.-W. Lee, H. Lee, L. Xie, X. Pan, R. A. De Souza, C.-B. Eom, and S. S. Nonnenmann, Sci. Adv. **5**, eaau8467 (2019).
[109]M. Lewin, C. Baeumer, F. Gunkel, A. Schwedt, F. Gaussmann, J. Wueppen, P. Meuffels, B. Jungbluth, J. Mayer, R. Dittmann, R. Waser, and T. Taubner, Adv. Funct. Mater. **28**, 1802834 (2018).
[110]W. Luo, M. Boselli, J.-M. Poumirol, I. Ardizzone, J. Teyssier, D. van der Marel, S. Gariglio, J.-M. Triscone, and A. B. Kuzmenko, Nat. Commun. **10**, 2774 (2019).
[111]F. Cordero, Phys. Rev. B **76**, 172106 (2007).
[112]D. V. Christensen, M. von Soosten, F. Trier, T. S. Jespersen, A. Smith, Y. Chen, and N. Pryds, Adv. Electron. Mater. **3**, 1700026 (2017).
[113]R. Meyer, A. F. Zurhelle, R. A. De Souza, R. Waser, and F. Gunkel, Phys. Rev. B **94**, 115408 (2016).
[114]N. H. Perry, J. J. Kim, S. R. Bishop, and H. L. Tuller, J. Mater. Chem. A **3**, 3602 (2015).
[115]D. V. Christensen, Y. Chen, V. Esposito, and N. Pryds, APL Mater. **7**, 013101 (2019).
[116]Y. Chen and R. J. Green, Adv. Mater. Interfaces **6**, 1900547 (2019).
[117]Y. Chen, N. Pryds, J. Kleibeuker, G. Koster, J. Sun, E. Stamate, B. Shen, G. Rijnders, and S. Linderoth, Nano Lett. **11**, 3774 (2011).
[118]L. Cao, O. Petracic, P. Zakalek, A. Weber, U. Ruecker, J. Schubert, A. Koutsioubas, S. Mattauch, and T. Brückel, Adv. Mater. **31**, 1806183 (2019).
[119]L. Yao, S. Inkinen, and S. van Dijken, Nat. Commun. **8**, 14544 (2017).
[120]C. Mitra, T. Meyer, H. N. Lee, and F. A. Reboredo, J. Chem. Phys. **141**, 084710 (2014).
[121]S. Bishop, D. Marrocchelli, C. Chatzichristodoulou, N. Perry, M. Mogensen, H. Tuller, and E. Wachsman, Annu. Rev. Mater. Res. **44**, 205 (2014).
[122]E. J. Crumlin, E. Mutoro, Z. Liu, M. E. Grass, M. D. Biegalski, Y. Lee, D. Morgan, H. M. Christen, H. Bluhm, and Y. Shao-Horn, Energy Environ. Sci. **5**, 6081 (2012).
[123]K. A. Stoerzinger, W. T. Hong, E. J. Crumlin, H. Bluhm, and Y. Shao-Horn, Acc. Chem. Res. **48**, 2976 (2015).
[124]M. Andrae, F. Dvorak, M. Vorokhta, S. Nemsak, V. Matolin, C. M. Schneider, R. Dittmann, F. Gunkel, D. N. Mueller, and R. Waser, APL Mater. **5**, 056106 (2017).
[125]C. Jooss, S. Mildner, M. Beleggia, D. Mierwaldt, and V. Roddatis, "ETEM studies of electrodes and electro-catalysts," in *Controlled Atmosphere Transmission Electron Microscopy: Principles and Practice*, edited by T. W. Hansen and J. B. Wagner (Springer International Publishing, Cham, 2016), pp. 301–329.
[126]S. Mildner, M. Beleggia, D. Mierwaldt, T. W. Hansen, J. B. Wagner, S. Yazdi, T. Kasama, J. Ciston, Y. Zhu, and C. Jooss, J. Phys. Chem. C **119**, 5301 (2015).
[127]T. Heisig, C. Baeumer, U. N. Gries, M. P. Mueller, C. L. Torre, M. Luebben, N. Raab, H. Du, S. Menzel, D. N. Mueller, C.-L. Jia, J. Mayer, R. Waser, I. Valov, R. A. D. Souza, and R. Dittmann, Adv. Mater. **30**, 1800957 (2018).